Chapter 7 Modeling of Thermoelectric Generators and Coolers with Heat Sinks

Contents

So far we have discussed the theories for thermoelectric generators and coolers. In this chapter, we develop a detailed mathematical model for a real thermoelectric generator system with heat sinks and also for a thermoelectric cooler system with heat sinks. We compare the model with measurements for verification, so that we can apply this model to other real thermoelectric systems.

7.1 Modeling of Thermoelectric Generators with Heat Sinks

We consider a real thermoelectric generator system with two commercial heat sinks as shown schematically in Figure 7.1 (a). We use the experimental input data shown in Table 7.1 for comparison purposes between modeling and measurements. Hot air flows by a blower through a hot heat sink while cold air flows through a cold heat sink by another blower. A commercial thermoelectric generator module is sandwiched between the hot and cold heat sinks as shown in Figure 7.1. A pair of thermocouples was installed on each side of the aluminium block to measure the junction temperature of the module. The hot and cold junction conductors are connected to an external resistance (not shown in the figure), so that the power output can be measured as the external resistance varies. The air volume flow rates are measured by pitot tubes to determine velocities in the hot and cold heat sinks. The input data and dimensions of the heat sinks, aluminium blocks, and the thermoelectric module are shown in Table 7.1. The concept of this experimental setup is to investigate a unit cell at a specific location of the entire system. We test only the unit cell and compare the experimental results with the present model. A schematic of the plate fin heat sinks is shown in Figure 7.1 (c).

Table 7.1 Experimental data for plate heat sinks, thermoelectric module, and aluminum block in a thermoelectric generator.

Description	**Values**	**Description**	**Values**
Hot air inlet temperature, $T_{\infty,h,in}$	61.6 ℃	**Thermoelectric Module (TE 127-1.0-2.5)**	
Cold air inlet temperature, $T_{\infty,c,in}$	22.6 ℃	Number of thermocouples, n	127
Air velocity in cold heat sink, V_c	9.834 m/s	Leg cross-sectional area, A_e	1.0 mm^2
Air velocity in hot heat sink, V_h	9.416 m/s	Leg length, L_e	2.5 mm
		Constant hot junction temperature, $T_{m,h}$	50 ℃
Plate fin heat sinks (UB30-20B, UB30-25B)		Max. current, I_{max}	1.9 A
Heat sink size (W × L × H mm)	30 × 30 × 20 (25)	Max. temp. difference, ΔT_{max}	79 ℃

Number of fins, n_s	14	Max. cooling power, Q_{cmax}	20.1 W
Fin spacing, z_s	1.53 mm	Max. voltage, V_{max}	15.9 V
Fin thickness, t_s	0.55 mm		
Profile length of cold heat sink, b_{sc}	20 mm	**Aluminum block**	
Profile length of hot heat sink, b_{sh}	25 mm	Size (W × L × H (t_{al}) mm)	30 × 30 × 19.1
Fin length, L_s	27 mm	Thermal conductivity, k_{al}	142 W/mK

Table 7.2 Air properties used in calculations.

Air Properties	At 300 K	At 330 K
Density	$\rho_c = 1.161\ kg/m^3$	$\rho_h = 1.05\ kg/m^3$
Specific heat	$c_{p,c} = 1007\ J/kgK$	$c_{p,h} = 1008\ J/kgK$
Kinematic viscosity	$\upsilon_c = 15.89 \times 10^{-6}\ m^2/s$	$\upsilon_h = 18.0 \times 10^{-6}\ m^2/s$
Thermal conductivity	$k_c = 0.0263\ W/mK$	$k_h = 0.028\ W/mK$
Prandtl number	$Pr_c = 0.707$	$Pr_h = 0.703$

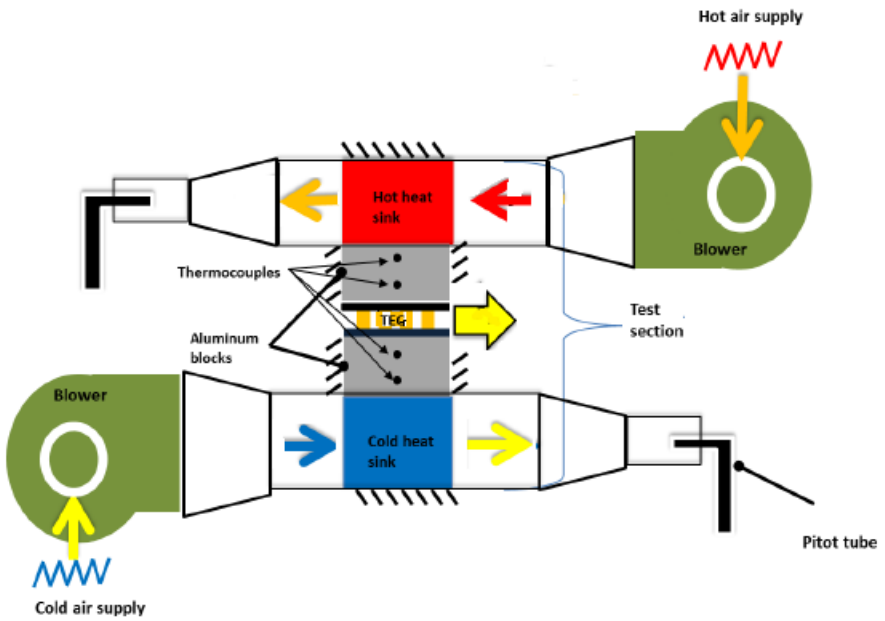

(a)

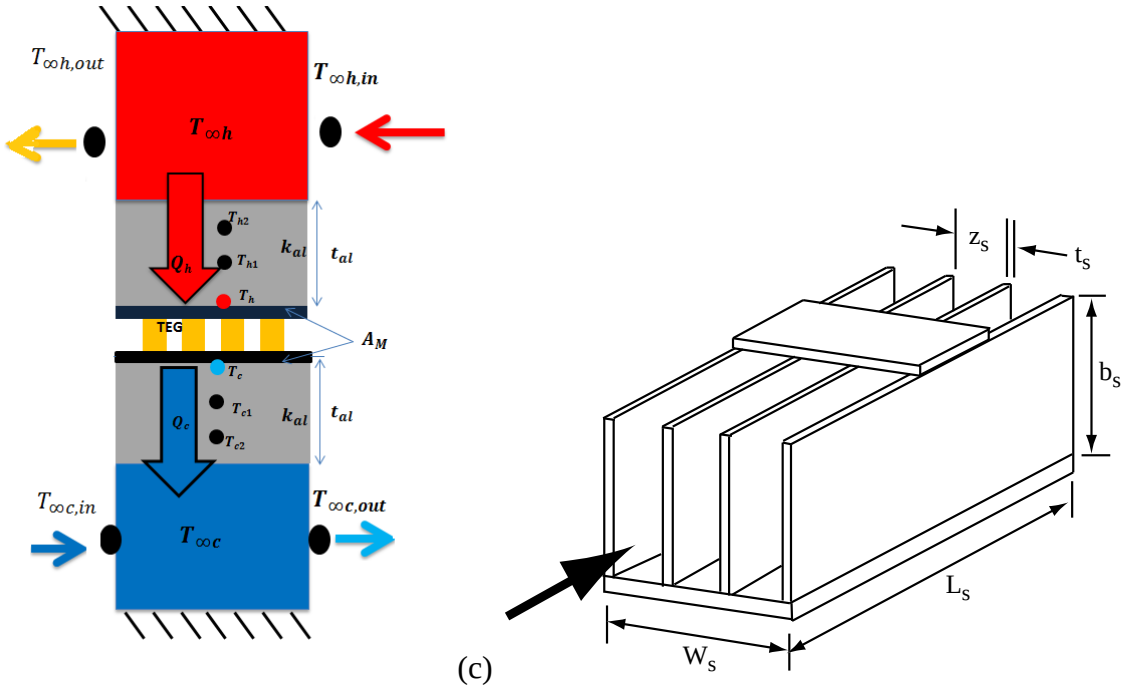

Figure 7.1 (a) Schematic of a real thermoelectric generator system with hot and cold flow channels including blowers, (b) a unit cell, and (c) a plate fin heat sink.

Modeling

Consider a steady-state one-dimensional heat flow from the hot air to the cold air in Figure 7.1 (a). We apply an enthalpy flow for the heat loss across the hot heat sink, where the heat loss must be absorbed into the heat sink by the Newton's law of cooling. We use the ideal equation with effective material properties for the thermoelectric module, which conceptually includes the effects of the thermal and electrical contact resistances as discussed in Chapter 2. We assume a linear temperature variation across the heat sink (this is a good assumption for a uniform heat crossflow), so that we can use the average of the hot inlet and outlet temperatures at the entry of heat sink. Then, the heat flow rate Q_h absorbed at the hot junction temperature T_h of the module and the heat flow rate Q_c liberated at the cold junction temperature T_c can be written in similar ways. The subscripts h and c denote the hot and cold quantities. Hence, we have the following heat balance equations as

$$\mathrm{Q}_h = \dot{m}_h c_{ph}\left(T_{\infty,h,in} - T_{\infty,h,out}\right) \tag{7.1}$$

$$\mathrm{Q}_h = \eta_{s,h} h_h A_{s,h}\left(\frac{T_{\infty,h,in} + T_{\infty,h,out}}{2} - T_h\right) \tag{7.2}$$

$$\mathrm{Q}_h = n\left[\alpha I T_h - \frac{1}{2} I^2 R_e + K_e(T_h - T_c)\right] \tag{7.3}$$

$$\mathrm{Q}_c = n\left[\alpha I T_c + \frac{1}{2} I^2 R_e + K_e(T_h - T_c)\right] \tag{7.4}$$

$$\mathrm{Q}_c = \eta_{s,c} h_c A_{s,c}\left(T_c - \frac{T_{\infty,c,in} + T_{\infty,c,out}}{2}\right) \tag{7.5}$$

$$\mathrm{Q}_c = \dot{m}_c c_{pc}\left(T_{\infty,c,out} - T_{\infty,c,in}\right) \tag{7.6}$$

where $\dot{m}$ is the mass flow rate, c_p the specific heat, η_s the entire heat sink efficiency (including the aluminum block), A_s the heat sink area, n the number of thermoelement couples, α the Seebeck coefficient, $\alpha = \alpha_p - \alpha_n$, $T_{\infty,h,in}$ the hot air inlet temperature, and $T_{\infty,c,in}$ the cold air inlet temperature. The internal resistance R_e is given by

$$R_e = \frac{\rho L_e}{A_e} \tag{7.7}$$

where ρ is the electrical resistivity, $\rho = \rho_n + \rho_p$. The thermal conductance K_e is given by

$$K_e = \frac{k A_e}{L_e} \tag{7.8}$$

where k is the thermal conductivity, $k = k_n + k_p$. There is one more equation needed for the solution, which is an expression for current I as

$$\mathrm{I} = \frac{\alpha(T_h - T_c)}{\frac{R_L}{n} + R_e} \tag{7.9}$$

where R_L is the external resistance, which is introduced in Chapter 2. Once we define all the operating conditions and material properties, we can solve the seven equations, (7.1) - (7.6) and (7.9), for seven unknowns, which are I, Q_h, Q_c, T_h, T_c, $T_{\infty,h,out}$, and $T_{\infty,c,out}$. Note that the hot and cold air outlet temperatures are the output results, not input data.

Heat Sink Area and Cross Flow Area for Heat Sinks

Using the dimensions in Table 7.1, we can calculate the heat sink areas and air flow areas for the heat sinks. The hot and cold heat sink areas (multiple fin areas) are

$$A_{s,h} = n_s\left[2(t_s + L_s)b_{s,h} + z_s L_s\right] = 0.020\ m^2 \tag{7.10}$$

$$A_{s,c} = n_s\left[2(t_s + L_s)b_{s,c} + z_s L_s\right] = 0.016\ m^2 \tag{7.11}$$

The hot and cold cross flow areas are

$$A_{cross,h} = n_s b_{s,h} z_s = 5.355\ cm^2 \tag{7.12}$$

$$A_{cross,c} = n_s b_{s,c} z_s = 4.284\ cm^2 \tag{7.13}$$

Mass Flow Rates

Using the air velocities in Table 7.1 and the air properties in Table 7.2, the mass flow rates for the hot and cold air flow are calculated as

$$\dot{m}_h = \rho_h V_h A_{cross,h} = 4.916\ g/s \tag{7.14}$$

$$\dot{m}_c = \rho_c V_c A_{cross,c} = 4.542 \ \ g/s \tag{7.15}$$

Convection Heat Transfer Coefficients

Using Equation (7.43) with the air velocities in Table 7.1, the reduced Reynolds numbers are

$$Re^*_{z,h} = \frac{V_h z_s}{\nu_h}\frac{z_s}{L_s} = 42.11 \tag{7.16}$$

$$Re^*_{z,c} = \frac{V_c z_s}{\nu_c}\frac{z_s}{L_s} = 49.82 \tag{7.17}$$

Since these values lie in the region of developing flow in Figure 7.8, we use Equation (7.41) for the forced convection in the heat sinks. The convection coefficients are

$$h_h = \frac{k_h}{z_s}\left[\left(\frac{Re^*_{z,h}Pr_h}{2}\right)^{-3} + \left(0.664\sqrt{Re^*_{z,h}}Pr_h^{\frac{1}{3}}\sqrt{1+\frac{3.65}{\sqrt{Re^*_{z,h}}}}\right)^{-3}\right]^{-1/3} = 86.68\frac{W}{m^2K} \tag{7.18}$$

$$h_c = \frac{k_c}{z_s}\left[\left(\frac{Re^*_{z,c}Pr_c}{2}\right)^{-3} + \left(0.664\sqrt{Re^*_{z,c}}Pr_c^{\frac{1}{3}}\sqrt{1+\frac{3.65}{\sqrt{Re^*_{z,c}}}}\right)^{-3}\right]^{-1/3} = 87.68\frac{W}{m^2K} \tag{7.19}$$

Single Fin Efficiencies

The single fin efficiencies for the hot and cold fins are calculated as

$$\eta_{f,h} = \frac{\tanh m_h b_{sh}}{m_h b_{sh}} = 0.70 \tag{7.20}$$

$$\eta_{f,c} = \frac{\tanh m_c b_{sc}}{m_c b_{sc}} = 0.78 \tag{7.21}$$

where

$$m_h = \sqrt{\frac{h_h 2(L_s + t_s)}{k_{al} L_s t_s}} = 47.59 \ \frac{1}{m} \tag{7.22}$$

$$m_c = \sqrt{\frac{h_c 2(L_s + t_s)}{k_{al} L_s t_s}} = 47.86 \ \frac{1}{m} \tag{7.23}$$

The single fin areas are calculated as

$$A_{f,h} = 2b_{sh}(L_s + t_s) = 1.377 \times 10^{-3} m^2 \tag{7.24}$$

$$A_{f,c} = 2b_{sc}(L_s + t_s) = 1.102 \times 10^{-3} m^2 \tag{7.25}$$

Overall Fin Efficiencies

Using Equation (7.10) and (7.11) for the multiple fin areas (heat sink areas), the overall fin efficiencies for the hot and cold heat sinks from Equation (7.55) are calculated as

$$\eta_{o,h} = 1 - n\frac{A_{f,h}}{A_{s,h}}\left(1 - \eta_{f,h}\right) = 0.707 \tag{7.26}$$

$$\eta_{o,c} = 1 - n\frac{A_{f,c}}{A_{s,c}}\left(1 - \eta_{f,c}\right) = 0.784 \tag{7.27}$$

Thermal Resistances of Heat Sink and Aluminum Block

Now we want to develop a total heat sink efficiency η_s including the aluminum blocks. Hence, we construct a thermal circuit between the average hot air temperature, $T_{\infty,h}$ and the hot junction temperature T_h, which is shown in Figure 7.2.

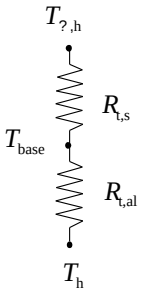

Figure 7.2 Thermal circuit between the average hot air temperature $T_{\infty,h}$ and the hot junction temperature T_h.

We introduce the entire efficiency η_s including both the heat sink and the aluminum block for simplicity. The entire thermal resistance is the sum of the heat sink resistance and the aluminum block resistance. The heat flow rate through the thermal circuit is

$$Q_h = \eta_{s,h} h_h A_{s,h} \left(T_{\infty,h} - T_h\right) = \frac{\left(T_{\infty,h} - T_h\right)}{\sum R_t} \tag{7.28}$$

where the entire thermal resistance is

$$\sum R_t = R_{t,s} + R_{t,al} = \frac{1}{\eta_{o,h} h_h A_{s,h}} + \frac{t_{al}}{k_{al} A_{al}} \tag{7.29}$$

which is expressed as

$$\frac{1}{\eta_{s,h} h_h A_{s,h}} = \frac{1}{\eta_{o,h} h_h A_{s,h}} + \frac{t_{al}}{k_{al} A_{al}} \tag{7.30}$$

If we multiply both sides by $h_h A_{s,h}$, we have the entire heat sink efficiency can be expressed by

$$\frac{1}{\eta_{s,h}} = \frac{1}{\eta_{o,h}} + \frac{h_h A_{s,h} t_{al}}{k_{al} A_{al}} \tag{7.31}$$

Hence, the entire heat sink efficiencies for the hot and cold air are

$$\eta_{s,h} = \left(\frac{1}{\eta_{o,h}} + \frac{h_h A_{s,h} t_{al}}{k_{al} A_{al}} \right)^{-1} = 0.598 \tag{7.32}$$

$$\eta_{s,c} = \left(\frac{1}{\eta_{o,c}} + \frac{h_c A_{s,c} t_{al}}{k_{al} A_{al}} \right)^{-1} = 0.674 \tag{7.33}$$

Note that the entire heat sink efficiencies are a little less than those of the overall fin efficiencies due to the thermal resistance of the aluminum blocks. This simplifies the analysis as shown in Equations (7.1) – (7.6).

Effective Material Properties

In order to solve those equations, we obviously need the material properties, which often requires a significant time and effort for system designers to obtain. A problem is that manufacturers of modules are not likely to provide those properties since they consider them proprietary information. We may measure the properties but there are still many uncertainties. The major uncertainties are the thermal and electrical contact resistances (manufacturability), the Thomson effect (temperature dependency of materials), and the radiation and convection losses.

We developed a technique [1] to resolve this problem, which is use of the effective material properties discussed in Chapter 2. We simply calculate the material properties from the maximum values of the module that are mostly provided by the manufacturers. We demonstrated that the technique works well in Chapter 2 for generators and in Chapter 3 for coolers. However, the present module is the thermoelectric cooler module, where the maximum parameters are

from the thermoelectric cooler. It turns out that the material properties can be obtained for either cooler or generator if the operating temperature is within a permissible range. Using the maximum cooler parameters in Table 7.1 and Equation (3.33), the effective figure of merit Z^* is calculated by

$$Z^* = \frac{2\Delta T_{max}}{\left(T_{m,h} - \Delta T_{max}\right)^2} = 2.651 \times 10^{-3} \frac{1}{K} \tag{7.34}$$

Using Equation (3.34), the effective Seebeck coefficient α^* is calculated by

$$\alpha^* = \frac{2Q_{cmax}}{nI_{max}\left(T_{m,h} + \Delta T_{max}\right)} = 414.27 \frac{\mu V}{K} \tag{7.35}$$

Using Equation (3.35), the effective electrical resistivity ρ^* is calculated by

$$\rho^* = \frac{\alpha^*\left(T_{m,h} - \Delta T_{max}\right) A_e/L_e}{I_{max}} = 2.129 \times 10^{-3} \Omega cm \tag{7.36}$$

Using Equation (3.36), the effective thermal conductivity k^* is calculated by

$$k^* = \frac{\alpha^{*2}}{\rho^* Z^*} = 3.041 \frac{W}{mK} \tag{7.37}$$

Note that the value of these effective material properties are the sum of *n*-type and *p*-type values, and will be anyhow used in Equations (7.1) – (7.6) and (7.9).

Comparison of Model and Measurements.

An experiment whose setup is shown schematically in Figure 7.1 was conducted using a variation of load resistance. The input data and the measured hot and cold junction temperatures,

current and voltage, and output power for the thermoelectric generator system are shown in Table 7.1. Most interesting is the measurement of the hot and cold junction temperatures, which are shown in Figure 7.3. The modeling involves many theoretical and empirical features such as the fin and heat sink efficiencies, an empirical correlation of the Nusselt number, the uncertainty of temperature measurement and its extrapolation, the effective material properties of the module, etc. Nevertheless, the comparison between the model and measurement in Figure 7.3 shows unexpectedly good agreement. It is interesting to note that, although the hot and cold inlet temperatures are constant, the hot and cold junction temperatures are no longer constant as seen in Figure 7.3. This is an important result in that the widely used analysis based on constant hot and cold junction temperatures may require some adjustment for this setup with heat sinks.

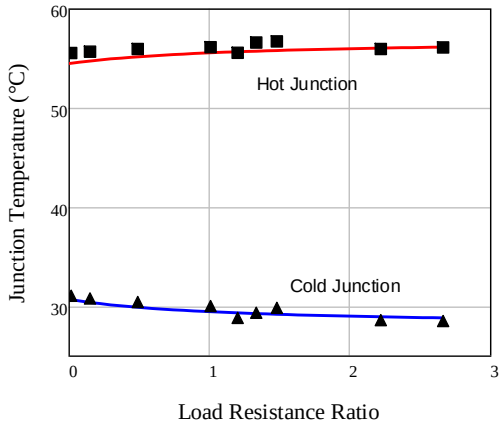

Figure 7.3 Hot and cold junction temperatures versus load resistance ratio with the hot and cold air inlet temperatures of 61.6 ℃ and 22.6 ℃, respectively.

The current and voltage measurements compared with the model prediction are shown in Figure 7.4. They are also in good agreement. Lastly, the output power is compared with measurement in Figure 7.5. As mentioned before, neither the measurement nor the prediction shows a load resistance ratio of $R_L/R_e = 1$ at the maximum output power, which is predicted with the constant hot and cold junction temperatures. If the temperature difference of the hot and cold air

inlet temperatures is high, the optimal load resistance ratio will be significantly greater than unity. This misunderstanding is often seen in the literature and industry.

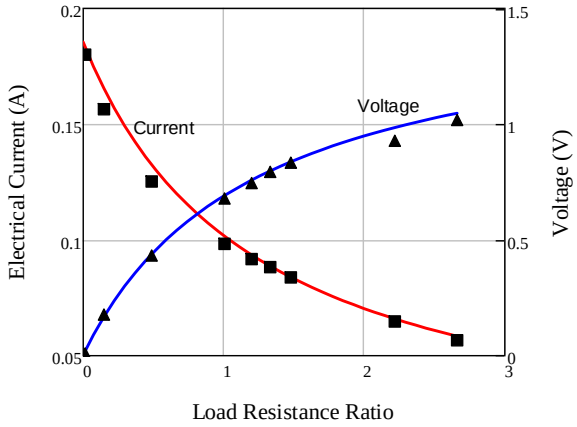

Figure 7.4 Electrical current and voltage versus load resistance at the hot and cold air inlet temperatures of 61.6 ℃ and 22.6 ℃, respectively. The symbols are measurements and the lines are predictions.

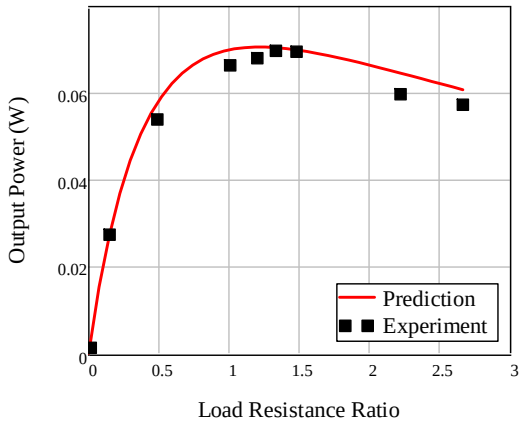

Figure 7.5 Output power versus load resistance ratio at the hot and cold air inlet temperatures of 61.6 ℃ and 22.6 ℃, respectively. The symbols are measurements and the lines are predictions.

Optimal Design of Heat Sink

We consider optimal design for the present thermoelectric generator system. First, we would like to see whether there is room for improvement in the fin design to maximize the heat flow at the given condition. We use Equations (7.48) and (7.49) to calculate the optimal fin thickness and the fin spacing as

$$t_{opt} = \left(\frac{2h_h}{k_{al}}\right)\left(\frac{b_{s,h}}{\beta}\right)^2 = 0.38\ mm \tag{7.38}$$

$$z_{opt} = L_s 3.24 Re_L^{-\frac{1}{2}} Pr_h^{-\frac{1}{4}} = 0.83\ mm \tag{7.39}$$

where the Reynolds number Re_L is calculated by

$$Re_L = \frac{V_h L_s}{\nu_h} = 1.31 \times 10^4 \tag{7.40}$$

The calculated optimal fin thickness of $t_{opt} = 0.38\ mm$ is less than the fin thickness of $t_s = 0.55\ mm$ in Table 7.1. And the calculated optimal fin spacing of $z_{opt} = 0.83\ mm$ is almost one half of the fin spacing of $z_s = 1.53\ mm$ in the table. Hence, it is believed that we can improve the design of the heat sink using the optimal values.

Optimal Design of Thermoelectric Module

We can check the optimal design of the thermoelectric module using a technique for optimal design developed in Chapter 4 [2]. We conducted the optimal design using the input data in Table 7.1, wherein the output power was plotted against the load resistance ratio along with the optimal design calculation in Figure 7.6. Two improvements are found: one is that the leg length can be reduced from the existing one (2.5 mm) to a shorter one (1.0 mm), the other is that $R_L/R_e = 1.36$. These result in about 16 % improvement in the output power in Figure 7.6.

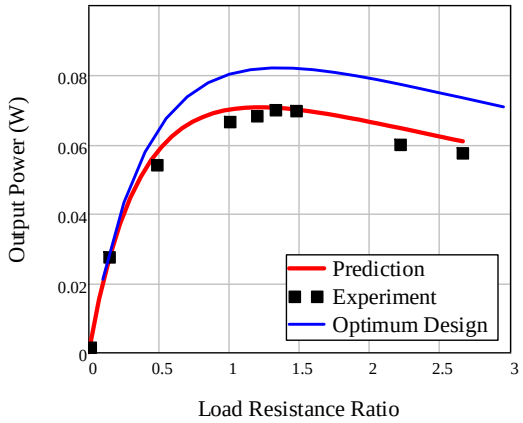

Figure 7.6 Output power versus load resistance ration with measurements, prediction and optimal design calculation.

7.2 Plate Fin Heat Sinks

We consider a typical plate fin heat sink as shown in Figure 7.7, where air flows within the channels.

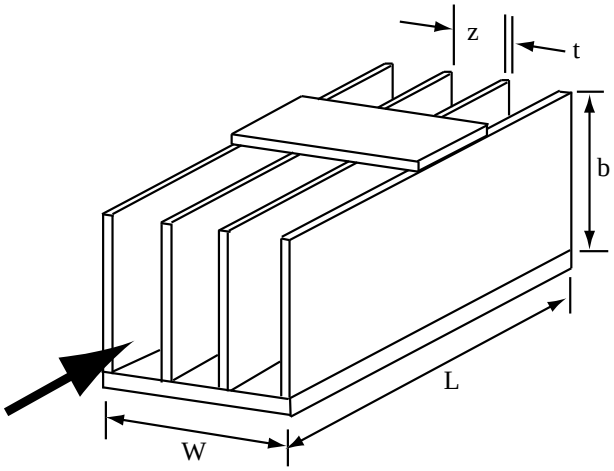

Figure 7.7 Schematic of plate fin heat sink

Nusselt Number for Air

The Nusselt number Nu_z for *plate fin heat sink* by forced convection in Figure 7.7 is developed by Teertstra et al. (1999) [3] with measurements, which is given as

$$Nu_z = \frac{hz}{k_f} = \left[\left(\frac{Re_z^* Pr}{2} \right)^{-3} + \left(0.664 \sqrt{Re_z^*} Pr^{\frac{1}{3}} \sqrt{1 + \frac{3.65}{\sqrt{Re_z^*}}} \right)^{-3} \right]^{-1/3} \tag{7.41}$$

where h is the convection coefficient and k_f the thermal conductivity of the fluid. The Reynolds number Re_z is defined with respect to fin spacing z and Pr is the Prandtl number. This equation covers the laminar and turbulent flows and also developing and fully-developed flows. There are two basic assumptions used in this equation. The one is that there is no "leakage" of air out the edge of the channels. This condition is achieved physically by placing a shroud on top of the fins as shown in Figure 7.7, such that all airflow is contained within the channels. The other is that $z \ll b$, such as in high aspect ratio manufactured heat sinks used for power electronics.

$$Re_z = \frac{Vz}{\nu} \tag{7.42}$$

where V is the air velocity in the channels, z the fin spacing, and ν the kinematic viscosity. The reduced Reynolds number Re_z^* is given as

$$Re_z^* = Re_z \frac{z}{L} \tag{7.43}$$

The experimental range of the reduced Reynolds number Re_z^* is given as

$$0.2 \leq Re_z^* \leq 200 \tag{7.44}$$

In Figure 7.8, the behaviour of two asymptotes from developing to fully-developed flow is seen, where the transition occurs in the region of about $Re_z^* = 10$. It is interesting to see that the larger fin spacing z in Equation (7.43) gives larger reduced Reynolds numbers which implies the developing flow.

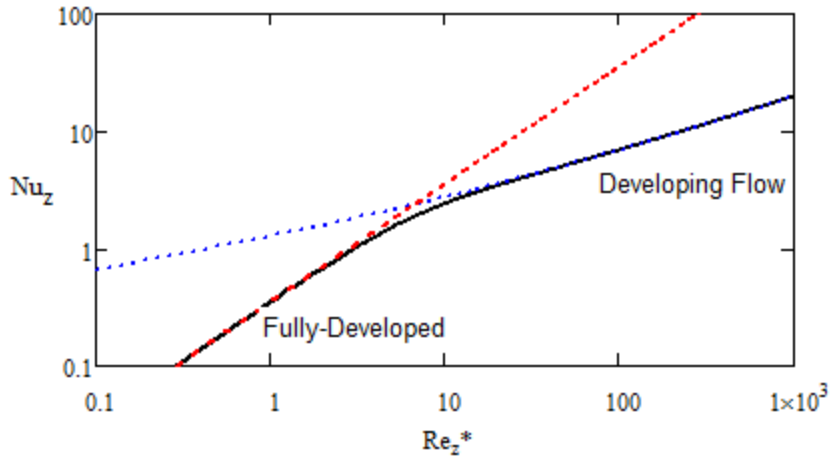

Figure 7.8 Nusselt number versus reduced Reynold number for developing and fully-developed flows.

Turbulent Flow for Gases and Liquids

The Nusselt number Nu_D for fully developed turbulent flow was studied by Gnielinski (1976) [4].

$$Nu_D = \frac{hD}{k_f} = \frac{(f/2)(Re_D - 1000)Pr}{1 + 12.7(f/2)^{1/2}(Pr^{2/3} - 1)} \tag{7.45}$$

where D is the hydraulic diameter of the channel and the Reynolds number Re_D is given as

$$Re_D = \frac{VD}{\nu} \tag{7.46}$$

The *Fanning friction coefficient* f for turbulent flow is given by

$$f = [1.58\, ln(Re_D) - 3.28]^{-2} \tag{7.47}$$

Optimal Design of Heat Sink

The optimal fin thickness and spacing are studied by Lee (2010) [5]. The optimal thickness t_s are approximated by assuming the single fin, which is given by

$$t_o = \left(\frac{2h}{k}\right)\left(\frac{b}{\beta}\right)^2 \tag{7.48}$$

where h is the convection coefficient, k the thermal conductivity of the fin, and b the profile length, and $\beta = 1.4192$, which is the optimal value for a single fin with a given profile length. However, this is assumed to be close enough to the optimal value of the multiple fins (see Lee (2010) for detail). The optimal fin spacing z_{opt} for forced convection is given by

$$\frac{z_{opt}}{L} = 3.24 Re_L^{-\frac{1}{2}} Pr^{-\frac{1}{4}} \tag{7.49}$$

where the Reynolds number Re_L is defined by

$$Re_L = \frac{VL}{\nu} \tag{7.50}$$

where L is the fin length in Figure 7.7.

Single Fin Efficiency

A single plate fin is considered for the fin efficiency as shown in Figure 7.9, where b is called the profile length, t_s is the fin thickness, h is the convection coefficient and L is the fin length. It is assumed that $T_{base} > T_\infty$. The profile area is $A_p = bt_s$, the cross-sectional area is $A_c = Lt_s$ and the perimeter is $P = 2(L + t_s)$. The single fin efficiency is given by [5]

$$\eta_f = \frac{\tanh mb}{mb} \tag{7.51}$$

where

$$m = \sqrt{\frac{hP}{kA_c}} = \sqrt{\frac{h2(L + t_s)}{kLt_s}} \tag{7.52}$$

The heat transfer rate q_f from the single fin using the fin efficiency η_f is

$$q_f = \eta_f h A_f (T_{base} - T_\infty) \tag{7.53}$$

where the single fin area A_f is given by

$$A_f = 2(L + t_s)b \tag{7.54}$$

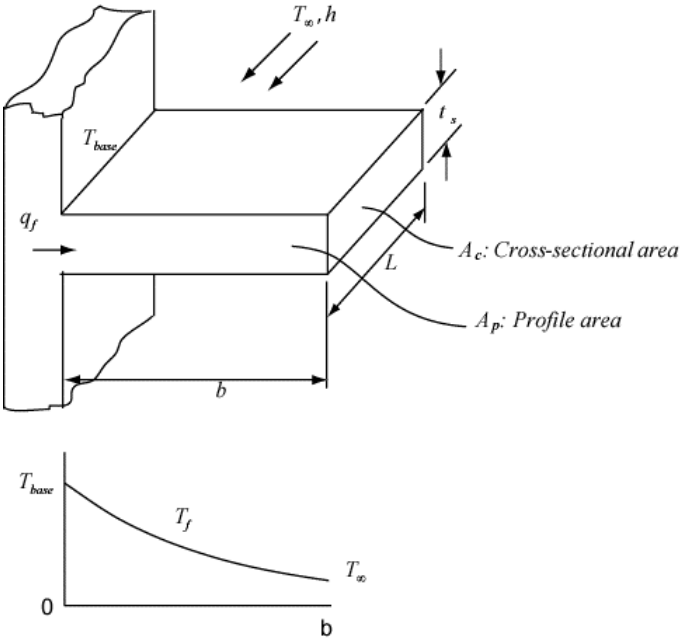

Figure 7.9 Single plate fin and the temperature distribution.

Overall Fin Efficiency

For a heat sink of multiple fins in Figure 7.7, the overall surface efficiency η_o is given by

$$\eta_o = 1 - n\frac{A_f}{A_s}(1 - \eta_f) \tag{7.55}$$

where n is the number of fins, A_f the single fin area, and A_s the total area of multiple fins (heat sink).

$$A_s = n[2(L + t_s)b + Lz] \tag{7.56}$$

The overall fin heat transfer rate q_s for a heat sink using the overall fin efficiency η_o is given by

$$q_s = \eta_o h A_s (T_{base} - T_\infty) \tag{7.57}$$

The overall fin efficiency η_o can be conveniently used to calculate the overall heat transfer rate q_s of a heat sink.

7.3 Modeling of Thermoelectric Coolers with Heat Sinks

We consider a real thermoelectric cooler system with two commercial heat sinks as shown schematically in Figure 7.10 for comparison purposes between modeling and measurements. Hot air flows by a blower through a heat sink while cold air flows through a heat sink by another blower. A commercial thermoelectric module is sandwiched between hot and cold heat sinks as shown. A pair of thermocouples was installed on each side of the aluminum block to measure the junction temperature of the module. The hot and cold junction conductors are connected to a current supply unit to measure the current and voltage. The air volume flow rates are measured by pitot tubes to measure the velocities in the hot and cold heat sinks. The input data and dimensions of the heat sinks, aluminum blocks, and the thermoelectric module are shown in Table 7.3. The air properties for the mean cold and hot temperatures are listed in Table 7.4. The concept of this experimental setup is to investigate a unit cell at a specific location of the entire system. We test only the unit cell and compare the experimental results with the present model. A schematic of the plate fin heat sinks is shown in Figure 7.10 (c).

Table 7.3 Experimental data for plate heat sinks, thermoelectric module, and aluminum block in a thermoelectric coolers.

Description	**Values**	**Description**	**Values**
Hot air inlet temperature, $T_{\infty,h,in}$	31.87 ℃	**Thermoelectric Module (C2-30-1503) (**W × L × H)	30 × 30 × 19.1 mm
Cold air inlet temperature, $T_{\infty,c,in}$	22.78 ℃	Number of thermocouples, n	127

Air velocity in cold heat sink, V_c	3.78 m/s	Leg cross-sectional area, A_e	1.21 mm^2
Air velocity in hot heat sink, V_h	5.42 m/s	Leg length, L_e	1.66 mm
		Constant hot junction temperature, $T_{m,h}$	50 ℃
Plate fin heat sinks (UB30-20B, UB30-25B)		Max. current, I_{max}	1.5 A
Heat sink size (W × L × H mm)	30 × 30 × 20 (25)	Max. temp. difference, ΔT_{max}	76 ℃
Number of fins, n_s	14	Max. cooling power, Q_{cmax}	37.4 W
Fin spacing, z_s	1.53 mm	Max. voltage, V_{max}	17.36 V
Fin thickness, t_s	0.55 mm		
Profile length of cold heat sink, b_{sc}	20 mm	**Aluminum block**	
Profile length of hot heat sink, b_{sh}	25 mm	Size (W × L × H (t_{al}) mm)	30 × 30 × 19.1
Fin length, L_s	27 mm	Thermal conductivity, k_{al}	142 W/mK

Table 7.4 Air properties used in calculations.

Air Properties	At 300 K	At 330 K
Density	$\rho_c = 1.161\ kg/m^3$	$\rho_h = 1.05\ kg/m^3$
Specific heat	$c_{p,c} = 1007\ J/kgK$	$c_{p,h} = 1008\ J/kgK$
Kinematic viscosity	$\upsilon_c = 15.89 \times 10^{-6}\ m^2/s$	$\upsilon_h = 18.0 \times 10^{-6}\ m^2/s$
Thermal conductivity	$k_c = 0.0263\ W/mK$	$k_h = 0.028\ W/mK$
Prandtl number	$Pr_c = 0.707$	$Pr_h = 0.703$

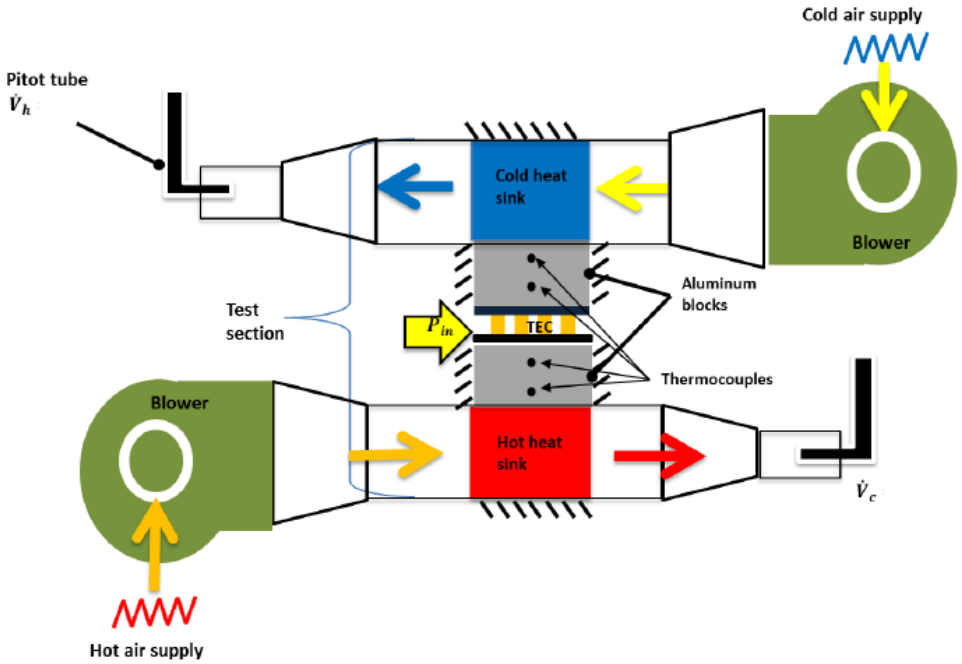

(a)

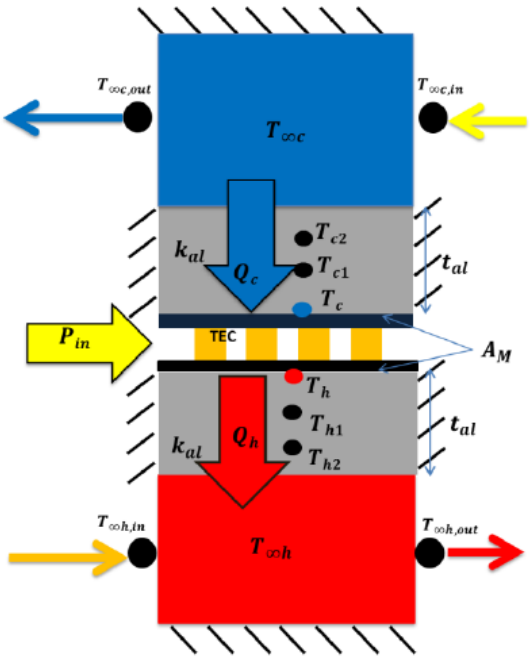

(b)

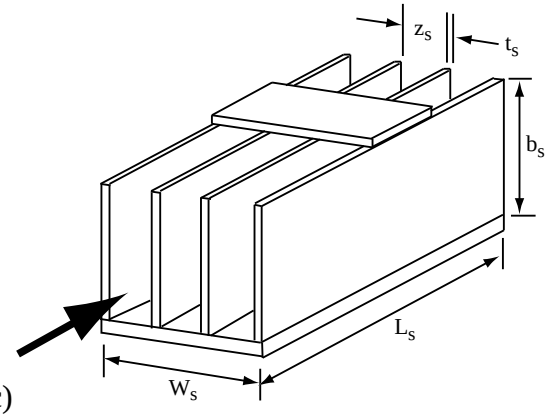

(c)

Figure 7.10 (a) Schematic of a real thermoelectric generator system with hot and cold flow channels, (b) a unit cell, and (c) a plate fin heat sink. Sketches from Attar (2015) [6].

Modeling

Consider a steady-state one-dimensional heat flow from the hot air to the cold air in Figure 7.10 (a). We apply an enthalpy flow for the heat loss across the hot heat sink, where the heat loss must be absorbed into the heat sink by the Newton's law of cooling. We use the ideal equation with effective material properties for the thermoelectric module, which conceptually includes the effects of the thermal and electrical contact resistances as discussed in Chapter 2. We assume a linear temperature variation across the heat sink (this is a good assumption for a uniform heat crossflow), so that we can use the average of the cold inlet and outlet temperatures at the entry of heat sink. Then, the heat flow rate Q_c absorbed at the cold junction temperature T_c of the module and the heat flow rate Q_h liberated at the cold junction temperature T_h can be written in similar ways. The subscripts h and c denote the hot and cold quantities. Hence, we have the following heat balance equations as

$$\mathrm{Q}_c = \dot{m}_c c_{pc}\left(T_{\infty,c,in} - T_{\infty,c,out}\right) \tag{7.58}$$

$$\mathrm{Q}_c = \eta_{s,c} h_c A_{s,c}\left(\frac{T_{\infty,c,in} + T_{\infty,c,out}}{2} - T_c\right) \tag{7.59}$$

$$\mathrm{Q}_c = n\left[\alpha I T_c - \frac{1}{2} I^2 R_e - K_e(T_h - T_c)\right] \tag{7.60}$$

$$\mathrm{Q}_h = n\left[\alpha I T_h + \frac{1}{2} I^2 R_e - K_e(T_h - T_c)\right] \tag{7.61}$$

$$\mathrm{Q}_h = \eta_{s,h} h_h A_{s,h}\left(T_h - \frac{T_{\infty,h,in} + T_{\infty,h,out}}{2}\right) \tag{7.62}$$

$$\mathrm{Q}_h = \dot{m}_h c_{ph}\left(T_{\infty,h,out} - T_{\infty,h,in}\right) \tag{7.63}$$

where $\dot{m}$ is the mass flow rate, c_p the specific heat, η_s the entire heat sink efficiency (including the aluminum block), A_s the heat sink area, n the number of thermoelement couples, α the

Seebeck coefficient, $\alpha = \alpha_p - \alpha_n$, $T_{\infty,h,in}$ the hot air inlet temperature, and $T_{\infty,c,in}$ the cold air inlet temperature. The internal resistance R_e is given by

$$R_e = \frac{\rho L_e}{A_e} \tag{7.64}$$

where ρ is the electrical resistivity, $\rho = \rho_n + \rho_p$. The thermal conductance K_e is given by

$$K_e = \frac{kA_e}{L_e} \tag{7.65}$$

where k is the thermal conductivity, $k = k_n + k_p$. Once we define all the operating conditions and material properties, we can solve the seven equations (7.58) - (7.63) for six unknowns, which are Q_h, Q_c, T_h, T_c, $T_{\infty,h,out}$, and $T_{\infty,c,out}$. Note that the cold and hot air outlet temperatures are the output results, not input data.

Heat Sink Area and Cross Flow Area for Heat Sinks

Using the dimensions in Table 7.3, we can calculate the heat sink areas and air flow areas for the heat sinks. The cold and hot heat sink areas (multiple fin areas) are

$$A_{s,c} = n_s\left[2(t_s + L_s)b_{s,c} + z_s L_s\right] = 0.016\ m^2 \tag{7.66}$$

$$A_{s,h} = n_s\left[2(t_s + L_s)b_{s,h} + z_s L_s\right] = 0.020\ m^2 \tag{7.67}$$

The cold and hot cross flow areas are

$$A_{cross,c} = n_s b_{s,c} z_s = 4.284\ cm^2 \tag{7.68}$$

$$A_{cross,h} = n_s b_{s,h} z_s = 5.355\ cm^2 \tag{7.69}$$

Mass Flow Rates

Using the air velocities in Table 7.3 and the air properties in Table 7.4, the mass flow rates for the cold and hot air flow are calculated as

$$\dot{m}_c = \rho_c V_c A_{cross,c} = 1.88\ g/s \tag{7.70}$$

$$\dot{m}_h = \rho_h V_h A_{cross,h} = 3.05\ g/s \tag{7.71}$$

Convection Heat Transfer Coefficients

Using Equation (7.43) with the air velocities in Table 7.3, the reduced Reynolds numbers are

$$Re^*_{z,c} = \frac{V_c z_s}{\nu_c}\frac{z_s}{L_s} = 20.63 \tag{7.72}$$

$$Re^*_{z,h} = \frac{V_h z_s}{\nu_h}\frac{z_s}{L_s} = 26.12 \tag{7.73}$$

Since these values lie in the region of developing flow in Figure 7.8, we use Equation (7.41) for the forced convection in the heat sinks. The convection coefficients are

$$h_c = \frac{k_c}{z_s}\left[\left(\frac{Re^*_{z,c} Pr_c}{2}\right)^{-3} + \left(0.664\sqrt{Re^*_{z,c}}\, Pr_c^{\frac{1}{3}}\sqrt{1+\frac{3.65}{\sqrt{Re^*_{z,c}}}}\right)^{-3}\right]^{-1/3} = 59.71\frac{W}{m^2 K} \tag{7.74}$$

$$h_h = \frac{k_h}{z_s}\left[\left(\frac{Re^*_{z,h}Pr_h}{2}\right)^{-3} + \left(0.664\sqrt{Re^*_{z,h}}Pr_h^{\frac{1}{3}}\sqrt{1+\frac{3.65}{\sqrt{Re^*_{z,h}}}}\right)^{-3}\right]^{-1/3} = 70.48\frac{W}{m^2K} \tag{7.75}$$

Single Fin Efficiencies

The single fin efficiencies for the cold and hot fins are calculated as

$$\eta_{f,c} = \frac{\tanh m_c b_{sc}}{m_c b_{sc}} = 0.83 \tag{7.76}$$

$$\eta_{f,h} = \frac{\tanh m_h b_{sh}}{m_h b_{sh}} = 0.74 \tag{7.77}$$

where

$$m_c = \sqrt{\frac{h_c 2(L_s + t_s)}{k_{al} L_s t_s}} = 39.50\ \frac{1}{m} \tag{7.78}$$

$$m_h = \sqrt{\frac{h_h 2(L_s + t_s)}{k_{al} L_s t_s}} = 42.91\ \frac{1}{m} \tag{7.79}$$

The single fin areas are calculated as

$$A_{f,c} = 2b_{sc}(L_s + t_s) = 1.102 \times 10^{-3} m^2 \tag{7.80}$$

$$A_{f,h} = 2b_{sh}(L_s + t_s) = 1.377 \times 10^{-3} m^2 \tag{7.81}$$

Overall Fin Efficiencies

Using Equation (7.10) and (7.11) for the multiple fin areas (heat sink areas), the overall fin efficiencies for the cold and hot heat sinks from Equation (7.55) are calculated as

$$\eta_{o,c} = 1 - n\frac{A_{f,c}}{A_{s,c}}\left(1 - \eta_{f,c}\right) = 0.840 \tag{7.82}$$

$$\eta_{o,h} = 1 - n\frac{A_{f,h}}{A_{s,h}}\left(1 - \eta_{f,h}\right) = 0.745 \tag{7.83}$$

Thermal Resistances of Heat Sink and Aluminum Block

Now we want to develop a total heat sink efficiency η_s including the aluminum blocks. Hence, we construct a thermal circuit between the average cold air temperature, $T_{\infty,c}$ and the cold junction temperature T_c, which is shown in Figure 7.11.

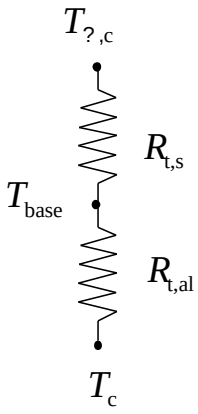

Figure 7.11 Thermal circuit between the average cold air temperature $T_{\infty,c}$ and the cold junction temperature T_c.

We introduce the entire efficiency η_s including both the heat sink and the aluminum block for simplicity. The entire thermal resistance is the sum of the heat sink resistance and the aluminum block resistance. The heat flow rate through the thermal circuit is

$$Q_c = \eta_{s,h} h_h A_{s,h} \left(T_{\infty,c} - T_c\right) = \frac{\left(T_{\infty,c} - T_c\right)}{\sum R_t} \tag{7.84}$$

where the entire thermal resistance is

$$\sum R_t = R_{t,s} + R_{t,al} = \frac{1}{\eta_{o,c} h_c A_{s,c}} + \frac{t_{al}}{k_{al} A_{al}} \tag{7.85}$$

which is expressed as

$$\frac{1}{\eta_{s,c} h_c A_{s,c}} = \frac{1}{\eta_{o,c} h_c A_{s,c}} + \frac{t_{al}}{k_{al} A_{al}} \tag{7.86}$$

If we multiply both sides by $h_c A_{s,c}$, we have the entire heat sink efficiency can be expressed by

$$\frac{1}{\eta_{s,c}} = \frac{1}{\eta_{o,c}} + \frac{h_c A_{s,c} t_{al}}{k_{al} A_{al}} \tag{7.87}$$

Hence, the entire heat sink efficiencies for the cold and hot air are

$$\eta_{s,c} = \left(\frac{1}{\eta_{o,c}} + \frac{h_c A_{s,c} t_{al}}{k_{al} A_{al}}\right)^{-1} = 0.75 \tag{7.88}$$

$$\eta_{s,h} = \left(\frac{1}{\eta_{o,h}} + \frac{h_h A_{s,h} t_{al}}{k_{al} A_{al}}\right)^{-1} = 0.644 \tag{7.89}$$

Note that the entire heat sink efficiencies are a little less than those of the overall fin efficiencies due to the thermal resistance of the aluminum blocks. This simplifies the analysis as shown in Equations (7.58) - (7.63).

Effective Material Properties

In order to solve those equations, we obviously need the material properties, which often requires a significant time and effort for system designers to obtain. A problem is that manufacturers of modules are not likely to provide those properties since they consider them proprietary information. We may measure the properties but there are still many uncertainties. The major uncertainties are the thermal and electrical contact resistances (manufacturability), the Thomson effect (temperature dependency of materials), and the radiation and convection losses.

We developed a technique [1] to resolve this problem, which is use of the effective material properties discussed in Chapter 3. We simply calculate the material properties from the maximum values of the module that are mostly provided by the manufacturers. We demonstrated that the technique works well in Chapter 3 for coolers. However, the present module is the thermoelectric cooler module, where the maximum parameters are from the thermoelectric cooler. Using the maximum cooler parameters in Table 7.3 Experimental data for plate heat sinks, thermoelectric module, and aluminum block in a thermoelectric coolers. and Equation (3.33), the effective figure of merit Z^* is calculated by

$$Z^* = \frac{2\Delta T_{max}}{\left(T_{m,h} - \Delta T_{max}\right)^2} = 2.651 \times 10^{-3} \frac{1}{K} \tag{7.90}$$

Using Equation (3.34), the effective Seebeck coefficient α^* is calculated by

$$\alpha^* = \frac{2Q_{cmax}}{nI_{max}\left(T_{m,h} + \Delta T_{max}\right)} = 414.27 \ \frac{\mu V}{K} \tag{7.91}$$

Using Equation (3.35), the effective electrical resistivity ρ^* is calculated by

$$\rho^* = \frac{\alpha^*\left(T_{m,h} - \Delta T_{max}\right) A_e / L_e}{I_{max}} = 2.129 \times 10^{-3} \Omega cm \tag{7.92}$$

Using Equation (3.36), the effective thermal conductivity k^* is calculated by

$$k^* = \frac{\alpha^{*2}}{\rho^* Z^*} = 3.041 \ \frac{W}{mK} \tag{7.93}$$

Note that the value of these effective material properties are the sum of *n*-type and *p*-type values, and will be anyhow used in Equations (7.58) - (7.63).

Comparison of Model and Measurements.

An experiment in which the setup is shown schematically in Figure 7.10 was conducted using a variation of current. The input data, the measured cold and hot junction temperatures and the cooling power and COP for the thermoelectric cooler system are shown in Table 7.3. Most interesting is the measurement of the cold and hot junction temperatures, which are shown in Figure 7.12. The modeling involves many theoretical and empirical features such as the fin and heat sink efficiencies, an empirical correlation of the Nusselt number, the uncertainty of temperature measurement and its extrapolation, the effective material properties of the module, etc. Nevertheless, the comparison between the model and measurement in Figure 7.12 shows unexpectedly good agreement. The coldest temperature of 12.16 ℃ occurs at I = 1.96 A, which is the maximum cooling power in the system. The calculated cooling power and COP versus current is compared with measurement in Figure 7.13 showing good agreement. The operating current is determined to have somewhere between the maximum COP and the maximum cooling power, depending on the applications.

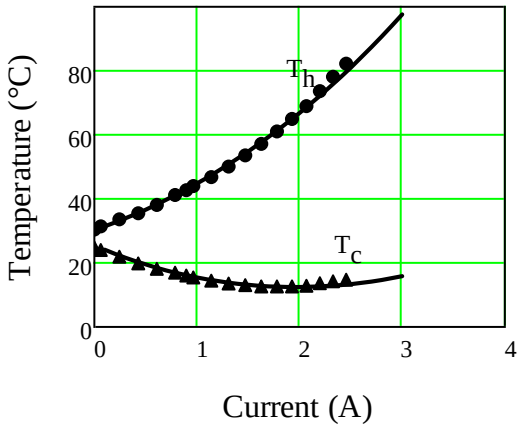

Figure 7.12 Cold and hot junction temperatures versus current with the cold and hot air inlet temperatures of 22.78 ℃ and 31.87 ℃, respectively. The symbols are measurements and the lines are predictions. Experimental data from Attar (2015) [6].

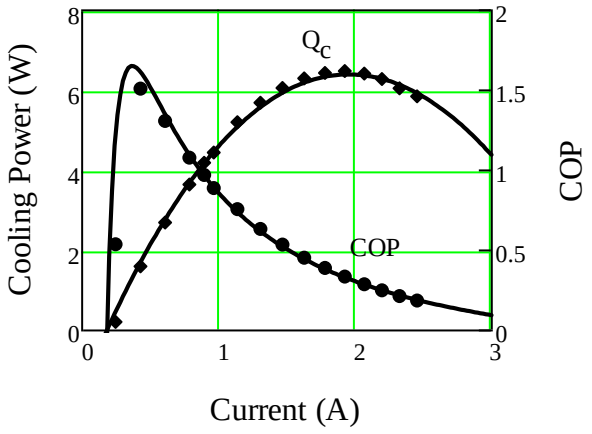

Figure 7.13 Calculated cooling power and COP as a function of current were compared with the measurements. The cold and hot air inlet temperatures of 22.78 ℃ and 31.87 ℃ were used in calculation. The symbols are measurements and the lines are predictions.

Conclusions

In conclusion, the present model reliably predicts both the thermoelectric generators and coolers as demonstrated in this chapter.

Problems

7.1 Develop a Mathcad program to compute the experimental data with the prediction (Figure 7.3, Figure 7.4, and Figure 7.5) using the input data in Table 7.1.

7.2 Develop a Mathcad program to provide Figure 7.6 and discuss the results.

References

1. Lee, H., A.M. Attar, and S.L. Weera, *Performance Prediction of Commercial Thermoelectric Cooler Modules using the Effective Material Properties.* Journal of Electronic Materials, 2015. **44**(6): p. 2157-2165.
2. Lee, H., *Optimal design of thermoelectric devices with dimensional analysis.* Applied Energy, 2013. **106**: p. 79-88.
3. Teertstra, P., et al. *Analytical forced convection modeling of plate fin heat sinks*. in *Fifteenth IEEE Semi-Therm Symposium*. 1999.
4. Gnielinski, V., *New equations for heat and mass transfer in turbulent pipe and channel flow*. Int. Chem. Eng., 1976. **16**: p. 359-368.
5. Lee, H., *Thermal Design; Heat Sink, Thermoelectrics, Heat Pipes, Compact Heat Exchangers, and Solar Cells*. 2010, Hoboken, New Jersey: John Wiley & Sons.
6. Attar, A., *Studying the Optimum Design of Automotive Thermoelectric Air Conditioning*, in *Mechanical and Aerospace Engineering*. 2015, PhD Thesis, Western Michigan University.